Analytical Prediction of Cogging Torque for Interior Permanent Magnet Synchronous Machines

Hooshang Mirahki[*] **and Mehdi Moallem**

Abstract—In this paper, a combination of Lumped-Parameters Model, Quasi-Poisson's equations and Conformal Mapping methods is used for predicting radial and tangential air gap flux density of Interior Permanent Magnet Synchronous Machine for calculation of cogging torque. In the proposed method, Lumped Parameters Model is used for calculation of saturation and flux leakage. Quasi-Poisson's equation is used for forming radial and tangential flux density in slotless stator, and finally Conformal Mapping is used to account for slot effects. Using the results of this method, cogging torque waveform can be calculated using Maxwell stress tensor and virtual work methods. To validate the method, results are compared with Finite Element Method results for a candidate Interior Permanent Magnet Synchronous Machine.

1. INTRODUCTION

Interior permanent magnet synchronous machines (IPMSMs) are used in different applications such as variable-speed drives, servo drives, electrical vehicles, and industrial drives due to their high efficiency, power density, power factor, and specific torque. IPMSMs have several advantages compared to Surface Permanent Magnet (SPM) machines, such as higher reluctance torque, wide constant power operating speed region, robust rotor structure, and immunity against demagnetization which make them a better choice than SPM machine in many applications, especially in high speed applications [1–3].

The main drawback of permanent magnet synchronous machines is the presence of cogging torque which is a result of interaction between rotor permanent magnet and stator slots and has no contribution to the average value of the electromagnetic torque. The cogging torque can lead to mechanical vibration, acoustic noise, extra stress on machine bearings, increase of cut-in speed of wind conversion systems, and other problems in drive systems [4, 5]. Therefore, researchers have always been looking for reducing cogging torque. A number of studies on cogging torque calculation and minimization can be found. Finite Element Method (FEM) and other numerical methods are used for cogging torque calculation in many papers [6, 7], and proper combination of the number of poles-number of stator slots [8], skewing of stator core or of permanent magnets [9], segmentation and shifting of PMs [10, 11], and proper calculation of pole arc width [9] are used for cogging torque reduction. However, since FEM is intensively time consuming, researchers have been always looking for analytical methods to ease the calculation of cogging torque [4, 12]. The analytical methods for calculation of cogging torque can be used in optimization process that needs thousands of iterations for finding an optimal solution. Analytical methods for cogging torque prediction are generally based on the torque calculation by Maxwell stress tensor or virtual work methods where the radial and tangential field components in the machine air gap are required [13].

Several methods have been proposed for slotless SPM machine which are based on solving Quasi-Poisson field equations directly and using conformal mapping for calculation of slots effect [14–17]. For IPMSM, however, solving Poisson equations is much more complicated due to the effect of saturation

* Corresponding author: Hooshang Mirahki (h.mirahki@ec.iut.ac.ir).
The authors are with the Department of Electrical and Computer Engineering, Isfahan University of Technology, Isfahan, Iran.

and IPMSM structural complexity [18, 19]. Therefore, for calculating air gap flux density in IPMSM, Lumped-Parameters Model (LPM) method seems to be the most promising approach [20]. In this method, we can calculate the average air gap flux density. Using this method, however, it is not possible to calculate the tangential field component and the precise profile of the field distribution. It is also not possible to calculate back-emf and cogging torque profile using LPM.

In this paper, combination of lumped parameter model, conformal mapping, and Quasi-Poissonian methods is used for accurate calculation of radial and tangential field components at the no-load condition. In the proposed method, LPM method is used for calculation of the field in the air gap of slotless stator. Then, the rotor of the IPMSM is substituted with a SPM machine rotor so that the field in the air gap remains unchanged. In the new machine (SPM), the remanent flux density, was calculated using LPM. Using the calculated of SPM machine and Poisson's equations, the radial and tangential air gap flux density in slotless rotor is calculated. Conformal mapping is used to take slots effect into consideration. Finally, we used radial and tangential components of the no-load air gap flux density and Maxwell stress tensor and virtual work methods for predicting cogging torque. Then acquired results are compared with Finite Element Method results which shows excellent accuracy.

2. CALCULATION OF FIELD COMPONENTS

For calculation and minimizing of cogging torque in PM machines either the virtual work or Maxwell stress tensor methods is used. According to equations presented in [3, 4, 21], for cogging torque calculation radial and tangential air gap flux density in the middle of air gap should be predicted. The principles of combining the closed form solution for the air gap flux density in an interior permanent magnet machine is described in [6]. Hence, in this paper the air gap field solution will be given without detailed derivation of all equations.

In this paper, for predicting radial and tangential components of air gap flux density, combination of three methods, lumped parameter model, conformal mapping, and Quasi-Poissonian equations methods is used. In this method, LPM is used for calculation of the field in the air gap of slotless stator of IPMSM. Then, the rotor of the IPMSM is substituted with the SPM machine rotor so that the field in the air gap remains unchanged. In the SPM machine, the remanent flux density, B_{rspm}, was calculated using LPM of surface permanent magnet machine. Using the calculated B_{rspm} in SPM machine and Poisson's equations, the radial and tangential air gap flux density in slotless rotor is calculated. Conformal mapping is used for taking slot effect into consideration.

2.1. Substituting IPMSM Rotor with SPM Rotor

In this part, IPMSM rotor is substituted with the rotor of SPM machine. In this process:

 (i) Air gap flux should be remained unchanged.

(ii) The inner and the outer radii of rotor and stator must be held fixed. Rotor of the IPMSM is substituted with rotor of SPM machine. The substituted rotor of SPM is consisted of a magnet with a width $l_{mspm} \ll g$ and pole-arc of α_1, where l_{mspm} is the magnet's width for SPM machine and α_1 is magnet's span.

Figure 1(a) shows a cross-section view of one-fourth of a six-pole IPMSM. Machine basic parameters are given in Table 1. Using flux line shown in Figure 1(a), lumped parameters model can be extracted as shown in Figure 1(b). Details of calculating air gap flux are given in [18, 22]. Using Kirchhoff's law and equations presented in [18], the air gap flux, φ_g, can be calculated with high accuracy. For simplicity, the reluctances of the rotor yoke and stator yoke can be easily ignored compared to the reluctance of the air gap.

Therefore, B_{rIPM} in IPMSM is substituted with the new B_{rspm} which is much larger than B_{rIPM}, since $l_{mspm} \ll g$. B_{rspm} is obtained from (1) which is obtained from the magnetic equivalent circuit of SPM machine shown in Figure 2(a). In this figure, the reluctance corresponding to the magnet's flux leakage is neglected because it is small.

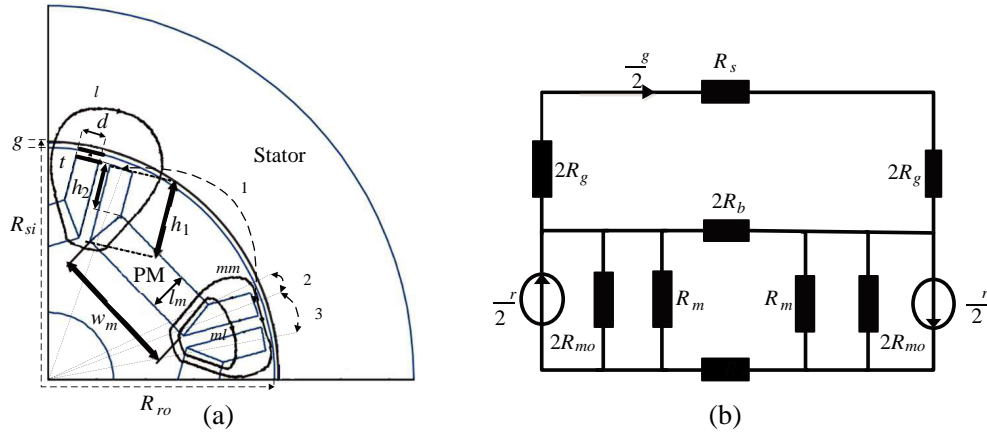$$B_{rspm} = \frac{\varphi_g}{A_{mspm}} \left(1 + \frac{R_g}{R_{mspm}}\right) \tag{1}$$

Figure 1. Structure and magnetic equivalent circuit of IPMSM. (a) IPMSM structure. (b) Magnetic equivalent circuit for IPMSM.

Table 1. IPM parameters.

Parameter	symbol	Quantity
Stator bore radius	R_s	47.5 [mm]
Air gap length	g	1 [mm]
Bridge width	t	1.5 [mm]
Flux barrier width	D	4 [mm]
Flux barrier height	h_1	15.32 [mm]
Flux barrier height	h_2	8.46 [mm]
Magnet width	w_m	27.7 [mm]
Magnet length	l_m	8.1 [mm]
Remanent flux density	B_{rIPM}	0.8 [T]
Saturation flux density	B_s	1.83 [T]
Pole pairs	p	3
Recoil permeability	μ_{rec}	1.05
Motor length	L	60 [mm]

$$R_{mspm} = \frac{l_{mspm}}{\mu_0 \mu_r A_{mspm}} \tag{2}$$

where B_{rspm} is the magnet remanence of the SPM machine, $A_{mspm} = \alpha_1 R_{ro} L$ is the area of SPM's magnet and R_{mspm} is the reluctance of SPM's magnet.

$$R_g = \frac{g}{\mu_0 A_g} \tag{3}$$

In the middle of air gap, $A_g = \alpha_p \frac{\pi(R_{si} - \frac{g}{2})}{p} L$, where $\alpha_p = \frac{\pi \alpha_1}{p}$ is the pole-arc to pole-pitch ratio. Figure 2(b) shows one pole of the SPM machine.

2.2. Calculation of Radial and Tangential Flux Density for SPM Machine

Zhu and Howe solved the quasi-Poissonian equations for calculation of the air gap radial and tangential flux density in a slotless SPM machine [14]. Hence, in this paper the air gap field solution will be given without detailed derivation of the equations. Note that the square radial magnetization in [14] is substituted with trapezoidal radial magnetization, as shown in Figure 3.
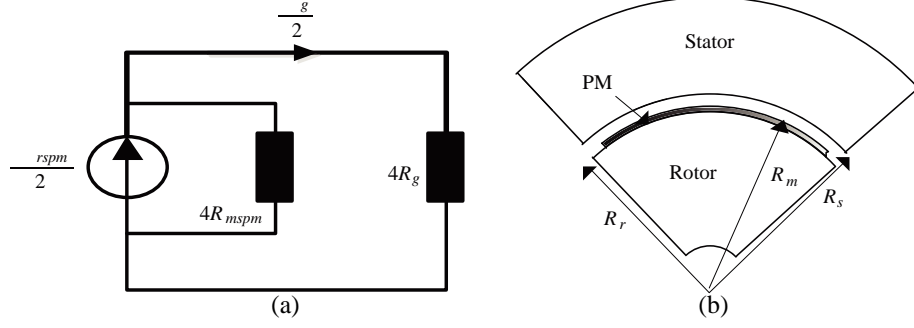
Figure 2. Structure and magnetic equivalent circuit of SPM machine. (a) Magnetic equivalent circuit for SPM machine as shown in Figure 2(b). (b) Substituted SPM machine.
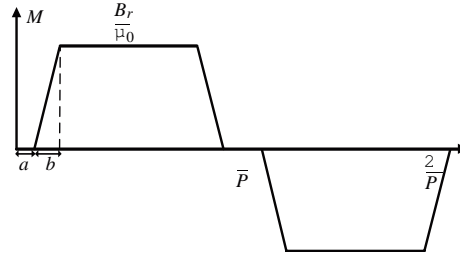

Figure 3. Magnetization distribution of inserted PM of SPM machine.

The Fourier series expansion of the signal in Figure 3 is given below:

$$\bar{M} = M_r \vec{r} = \sum_{n=1,3,5,\ldots}^{\infty} M_n \sin(np\theta) \cdot \vec{r} \tag{4}$$

$$M_r = \frac{-2B_{rspm}}{\mu_0 b\pi n^2}[\sin(an)\{1-(-1)^n\} + \sin(n[a+b])\{-1+(-1)^n\}] \tag{5}$$

$$M_n = \sum_{n=1,3,5,\ldots}^{\infty} \frac{-2B_{rspm}}{\mu_0 b\pi n^2}[\sin(an) - \sin(n(a+b))]\sin(np\theta) \tag{6}$$

where $a = -\alpha_3 \cdot p$, $b = 2\alpha_2 \cdot p$, and p is number of pole pairs. Solving simultaneous Laplace's equation in air gap and Quasi-Poisson's equations in the permanent magnet, radial and tangential air gap flux density can be calculated. Details of field calculation in the middle of air gap for slotless SPM machine is described in [16]:

$$B_{rn}(r) = \sum_{n=1,3,5,\ldots}^{\infty} \frac{\mu_0 M_n}{\mu_r} \frac{np}{(np)^2 - 1} \cdot \left[\left(\frac{r}{R_s}\right)^{np-1}\left(\frac{R_m}{R_s}\right)^{np+1} + \left(\frac{R_m}{r}\right)^{np+1}\right]$$

$$\cdot \left\{ \frac{(np-1) + 2\left(\frac{R_r}{R_m}\right)^{np+1} - (np+1)\left(\frac{R_r}{R_m}\right)^{2np}}{\frac{\mu_r+1}{\mu_r}\left[1 - \left(\frac{R_r}{R_s}\right)^{2np}\right] - \frac{\mu_r-1}{\mu_r}\left[\left(\frac{R_m}{R_s}\right)^{2np} - \left(\frac{R_r}{R_m}\right)^{2np}\right]} \right\} \tag{7}$$

$$B_{\theta n}(r) = \sum_{n=1,3,5,\ldots}^{\infty} \frac{\mu_0 M_n}{\mu_r} \frac{np}{(np)^2 - 1} \cdot \left[-\left(\frac{r}{R_s}\right)^{np-1}\left(\frac{R_m}{R_s}\right)^{np+1} + \left(\frac{R_m}{r}\right)^{np+1}\right]$$

$$\cdot \left\{ \frac{(np-1) + 2(\frac{R_r}{R_m})^{np+1} - (np+1)(\frac{R_r}{R_m})^{2np}}{\frac{\mu_r+1}{\mu_r}[1 - (\frac{R_r}{R_s})^{2np}] - \frac{\mu_r-1}{\mu_r}\left[\left(\frac{R_m}{R_s}\right)^{2np} - \left(\frac{R_r}{R_m}\right)^{2np}\right]} \right\} \tag{8}$$

where R_s, R_m, R_r are radii of SPM machine as shown in Figure 2(b).

2.2.1. Slots Effect for New SPM Machine

To account for slots effect, conformal mapping is used. According to [4], the flux density in the slotted air gap of a surface mounted PM motor can be written as:

$$B_s(r, \theta, \alpha) = B_{sr}(r, \theta, \alpha) + jB_{s\theta}(r, \theta, \alpha) = [B_r(r, \theta, \alpha) + jB_\theta(r, \theta, \alpha)] \times [\lambda_a(r, \theta) - j\lambda_b(r, \theta)] \quad (9)$$

where B_{sr} and $B_{s\theta}$ are radial and tangential flux density components in the slotless air gap, and λ_a and λ_b are the real and imaginary components of the complex relative air-gap permeance. The $B_{sr}(r, \theta, \alpha)$, $B_{s\theta}(r, \theta, \alpha)$, $\lambda_a(r, \theta)$, and $\lambda_b(r, \theta)$ along a circular arc inside the air gap can be written in the form of Fourier series:

$$
\begin{aligned}
B_r(r, \theta, \alpha) &= \sum_n B_{rn}(r) \cos[np(\theta - \alpha)] \\
B_\theta(r, \theta, \alpha) &= \sum_n B_{\theta n}(r) \sin[np(\theta - \alpha)] \\
\lambda_a(r, \theta) &= \lambda_0(r) + \sum_m \lambda_{am}(r) \cos(mQ_s\theta) \\
\lambda_b(r, \theta) &= \sum_m \lambda_{bm}(r) \sin(mQ_s\theta)
\end{aligned}
\quad (10)
$$

where r is the radius in the middle of air gap, $\alpha = \omega_{rm}t$ is the angular position of the rotor and ω_{rm} is the mechanical rotor speed in rad/s and t is time. Also $B_{rn}(r)$ and $B_{\theta n}(r)$ are described in Equations (7) and (8), respectively. The complex relative air-gap permeance is found by transforming the actual slotted air gap into a slotless air gap using four conformal transformations, as shown in Figure 4(a). The S plane contains the original slot geometry (Figure 4(b)), and the K plane contains the slotless air gap (Figure 4(c)), while Z, W, and K planes are used for intermediate transformations. Base on the results presented in [4], without detailed derivation of the equations, we have:

$$T_1: s = e^z, \quad s = r\cos(\theta) + jr\sin(\theta), \quad r = R_s - g/2 \tag{11}$$

$$T_2: z = j\frac{g'}{\pi}\left[\ln\left|\frac{1+p}{1-p}\right| - \ln\left|\frac{u+p}{u-p}\right|\right] - \frac{2(u-1)}{\sqrt{u}}\arctan\left(\frac{p}{\sqrt{u}}\right) + \ln(R_s) + j\theta_s + j\theta_2 \quad \left(p = \sqrt{\frac{w-u}{w-v}}\right) \tag{12}$$

$$T_3: t = j\frac{g'}{\pi}\ln(w) + \ln(R_s) + j\frac{\theta_s}{2} \tag{13}$$

$$T_4: k = e^t \tag{14}$$

where, the coefficients u and v are $u = [\frac{b'_0}{(2g')} + \sqrt{(\frac{b'_0}{2g'})^2 + 1}]^2$, $v = \frac{1}{u}$, $g' = \ln\frac{R_s}{R_r}$, $b'_0 = \theta_2 - \theta_1$. The link between S and K planes is $B_s = B_k(\frac{\partial K}{\partial S})^* = B_k(\frac{\partial K}{\partial t} \cdot \frac{\partial t}{\partial w} \cdot \frac{\partial w}{\partial z} \cdot \frac{\partial z}{\partial s})^*$, so the flux density is:

$$B_s = B_k\left[\frac{k}{s}\frac{(w-1)}{(w-v)^{0.5}(w-u)^{0.5}}\right]^* \tag{15}$$

The flux density B_k with its real and imaginary parts B_r and B_θ represents the field solution in the slotless air gap given by (7), (8), and (10).

As an example, the field solution in the middle of the air gap ($r = R_{si} - g/2$) for the six-pole interior permanent magnet synchronous machine is calculated using above method. The machine parameters are given in Table 1. The radial and tangential air gap flux density considering the stator's slot effect can be calculated using Equation (15). Figure 5(a) and Figure 5(b) show the radial and tangential air gap flux density for the interior permanent magnet synchronous machine using the analytical method and finite element method which are in great agreement.
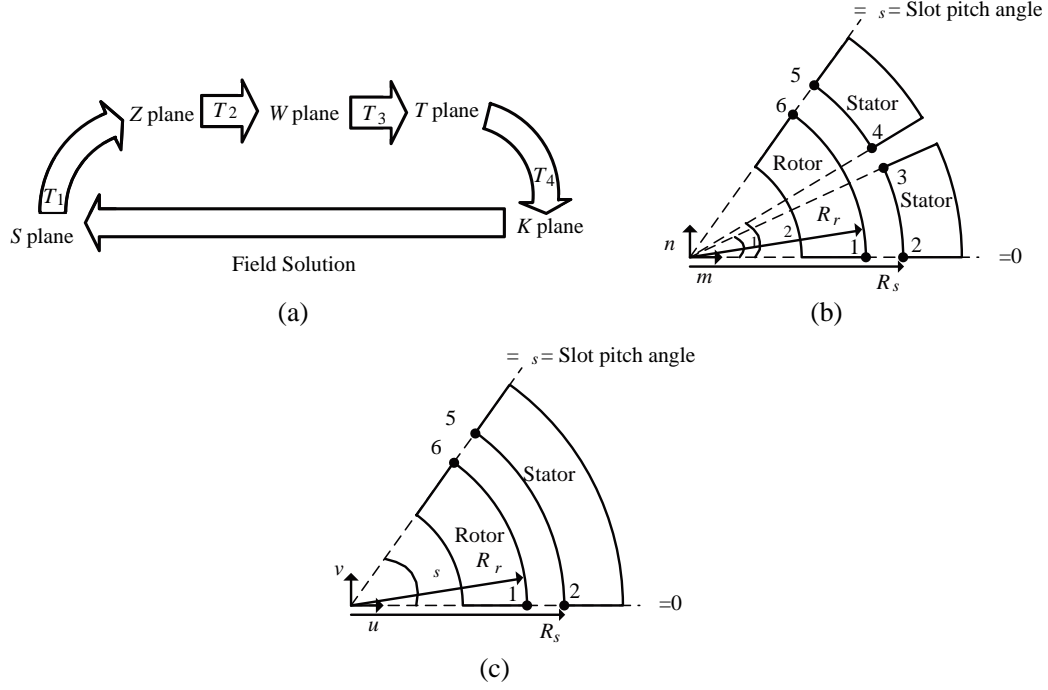
Figure 4. Basic transformation and shape of slot in the S and K plane. (a) Basic transformation required for conformal mapping. (b) Single infinitely deep slot opening in the S plane. (c) Slot opening in the K plane (slotless air gap).
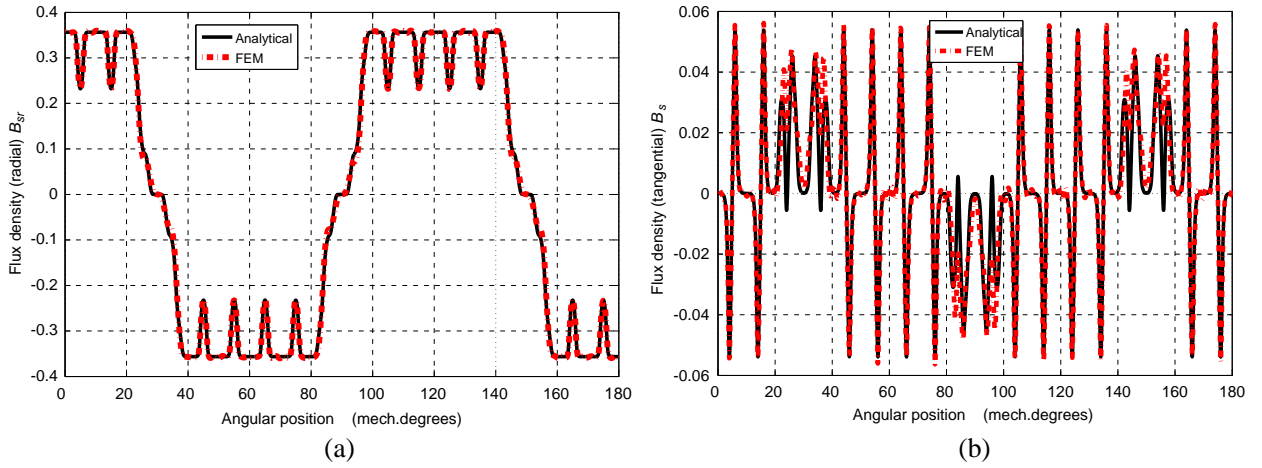

Figure 5. Waveforms of the radial and tangential flux density in the middle of the air gap of IPMSM. (a) Waveforms of the radial flux density in the middle of the air gap of a slotted IPMSM. (b) Waveforms of the tangential flux density in the middle of the air gap of a slotted IPMSM.

3. COGGING TORQUE CALCULATION BASED ON MAXWELL STRESS AND VIRTUAL WORK METHODS

Using field components in previous section cogging torque can be calculated. In virtual work method radial component field is used for calculating the cogging torque. In this method, the energy stored in

air gap W_{airgap} (in joules) can be calculated as a function of the rotor angle θ as follows:

$$W_{airgap}(\alpha) = \frac{L(R_s^2 - R_m^2)}{4\mu_0} \times \int_0^{2\pi} B_r^2(r, \theta, \alpha)\lambda_a^2(r, \theta)d\theta \tag{16}$$

where R_s and R_m are the inner radius of the stator core and outer radius of magnets of SPM machine [m]. μ_0 is the permeability of air [H/m], B_r the radial component of the flux density in slotless air gap, and λ_a the real component of the complex relative air gap permeance. The cogging torque T_{cog} can be calculated as follows:

$$T_c(\alpha) = -\frac{\partial W_{airgap}(\alpha)}{\partial \alpha} \tag{17}$$

In Maxwell stress tensor method radial and tangential field components are used for calculating torque. According to equations presented in [21], the torque equation in the integral form can be written as:

$$T_c(\alpha) = \frac{1}{\mu_0}Lr^2 \int_0^{2\pi} B_{sr}(r, \theta, \alpha)B_{s\theta}(r, \theta, \alpha)d\theta \tag{18}$$

where B_{sr}, and $B_{s\theta}$ are the radial and tangential components of the flux density in the slotted air gap of the surface PM motor.

For FE analysis, the time stepping transient method with moving air gap is used. The cogging torque of the candidate machine can be calculated from the virtual work based on the energy of the moving air gap [23]. Since cogging torque values are small and can be effected by numerical errors of mesh, therefore, the length of air gap is divided into 10 layers. Figure 6(a) shows the meshed FE model and Figure 6(b) shows enlarge detail of the mesh in the vicinity of the slot opening.

Using this method, the cogging torque is calculated for three different slot openings. Figures 7(a)–(c) show for the variation of cogging torque versus mechanical degree for the analytical methods (Maxwell stress tensor and virtual work) and finite element method for $b_0 = 1$ [mm], $b_0 = 2$ [mm], and $b_0 = 3$ [mm].

The cogging torque waveform calculated using Maxwell stress tensor for three different slot openings show better results than virtual work method as compared with FEM. Conformal mapping method presented in [4], assumes no shape deformation in the magnets and a circular path to predict the field components. However, slightly deforms the shape of magnet and circular path in the K plane. Hence, the assumption will result in errors in predicted air gap filed components. Since interaction between the magnet edges and the slot opening is decisive for cogging torque waveform shape, any errors in the air gap flux density prediction affects the cogging torque calculation as well. In this method, due to the
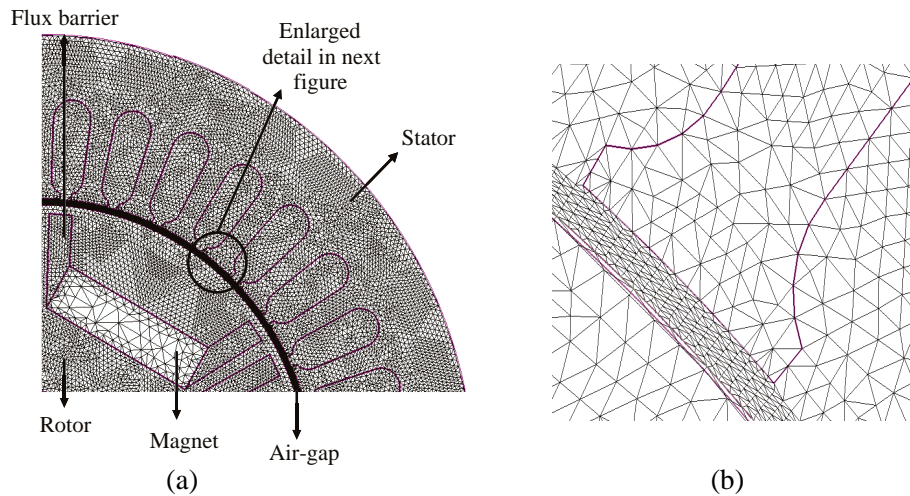

Figure 6. Finite element mesh. (a) Meshed finite element model of the one pole of IPMSM. (b) Enlarged detail of the finite element mesh.
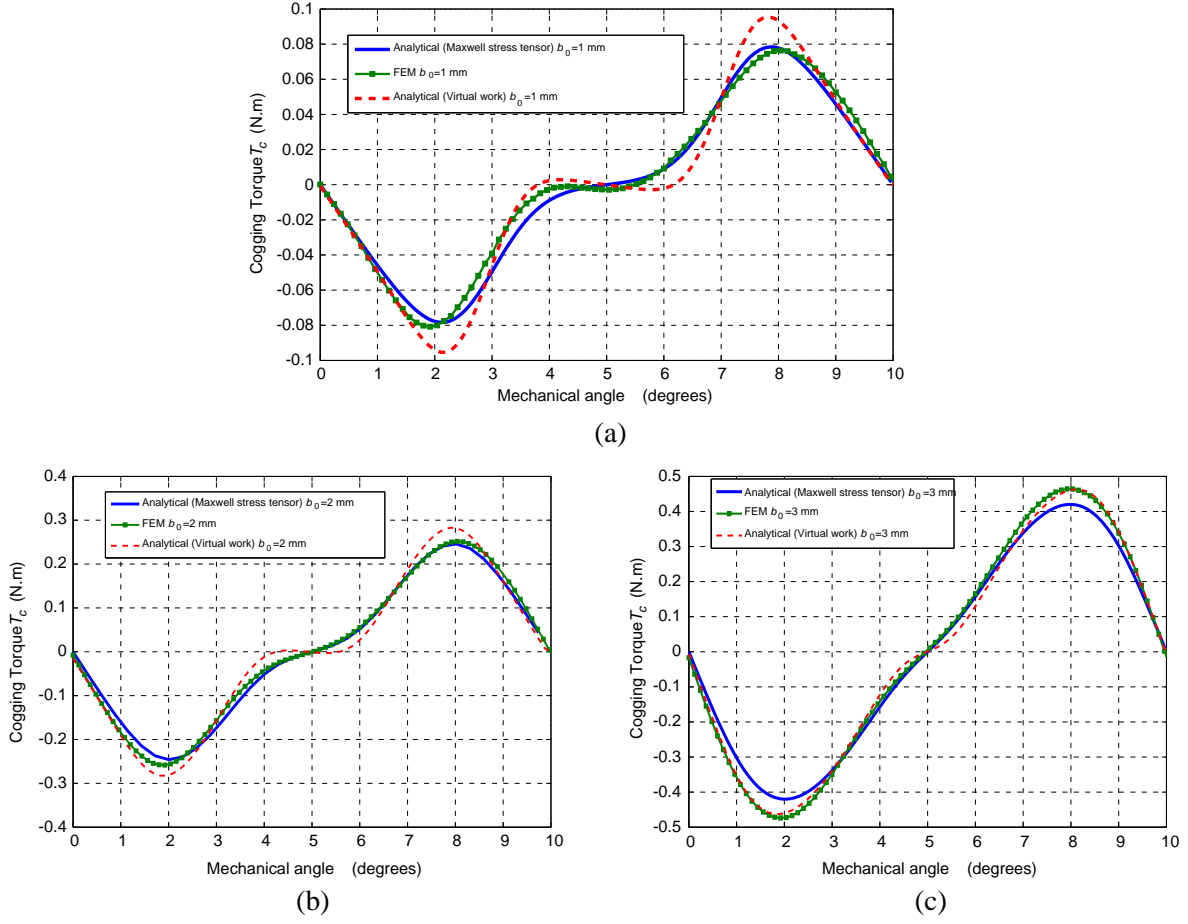
Figure 7. Comparison of cogging torque. (a) Comparison of cogging torque waveform for $b_0 = 1\,\text{mm}$. (b) Comparison of cogging torque waveform for $b_0 = 2\,\text{mm}$. (c) Comparison of cogging torque waveform for $b_0 = 3\,\text{mm}$.

small magnet width compared with air gap width in new SPM machine, no shape deformation can be assumed in magnets in the K plane.

In virtual work method, since is only used radial air gap flux density for calculating cogging torque, therefore, this method has more error than Maxwell stress tensor. This error includes cogging torque shape and maximum amplitude. The cogging torque predicted using virtual work method show importance of the accuracy of tangential air gap flux density in interior permanent magnet synchronous machine.

4. CONCLUSION

In this paper, a new method is proposed, which combines the Lumped-Parameters Model, Quasi-Poisson's equations, and Conformal Mapping which yields an accurate estimate of radial and tangential air gap flux density for interior permanent magnet synchronous machine. Using radial and tangential air gap flux density from this method, cogging torque waveform is predicted using Maxwell stress tensor and virtual work methods. The validity of the proposed method is verified by comparing its results with that obtained from finite element method. The proposed method is proved to be accurate for calculations of the interior permanent magnet synchronous machine's no-load performance characteristics. Using the proposed method for machine's optimization, which requires many machine analysis, is much faster than using Finite Element Method.

REFERENCES

1. Miller, T. M. E., *Brushless Permanent-magnet and Reluctance Motor Drives*, Oxford University Press, New York, 1989.

2. Boldea, I., *Reluctance Synchronous Machines and Drives*, Oxford University Press, New York, 1996.

3. Wu, L. J., Z. Zhu, D. Staton, M. Popescu, and D. Hawkins, "Comparison of analytical models of cogging torque in surface-mounted pm machines," *IEEE Transactions on Industrial Electronics*, Vol. 59, No. 6, 2414–2425, 2012.

4. Zarko, D., D. Ban, and T. Lipo, "Analytical solution for cogging torque in surface permanent-magnet motors using conformal mapping," *IEEE Trans. Mag.*, Vol. 44, No. 1, 52–65, 2008.

5. Dosiek, L. and P. Pillay, "Cogging torque reduction in permanent magnet machines," *IEEE Transactions on Industry Applications*, Vol. 43, No. 6, 1565–1571, 2007.

6. Mirahki, H., M. Moallem, and S. A. Rahimi, "Design optimization of IPMSM for 42 V integrated starter-alternator using lumped parameter model and genetic algorithms," *IEEE Trans. Mag.*, Vol. 50, No. 3, 114–119, 2014.

7. Parsa, L. and L. Hao, "Interior permanent magnet motors with reduced torque pulsation," *IEEE Transactions on Industrial Electronics*, Vol. 55, No. 2, 602–609, 2008.

8. Dorrell, D. and M. Popescu, "Odd stator slot numbers in brushless DC machines — An aid to cogging torque reduction," *IEEE Trans. Mag.*, Vol. 47, No. 10, 3012–3015, 2011.

9. Bianchi, N. and S. Bolognani, "Design techniques for reducing the cogging torque in surface-mounted PM motors," *IEEE Transactions on Industry Applications*, Vol. 38, No. 5, 1259–1265, 2002.

10. Boukais, B. and H. Zeroug, "Magnet segmentation for commutation torque ripple reduction in a brushless DC motor drive," *IEEE Trans. Mag.*, Vol. 46, No. 11, 3909–3919, 2010.

11. Ashabani, M. and Y. A. R. I. Mohamed, "Multiobjective shape optimization of segmented pole permanent-magnet synchronous machines with improved torque characteristics," *IEEE Trans. Mag.*, Vol. 47, No. 4, 795–804, 2011.

12. Zhu, L., S. Z. Jiang, Z. Q. Zhu, and C. C. Chan, "Analytical methods for minimizing cogging torque in permanent-magnet machines," *IEEE Trans. Mag.*, Vol. 45, No. 4, 2023–2031, 2009.

13. El-Refaie, A., T. Jahns, and D. Novotny, "Analysis of surface permanent magnet machines with fractional-slot concentrated windings," *IEEE Transactions on Energy Conversion*, Vol. 21, No. 1, 34–43, 2006.

14. Zhu, Z., D. Howe, E. Bolte, and B. Ackermann, "Instantaneous magnetic field distribution in brushless permanent magnet dc motors. Part I. Open-circuit field," *IEEE Trans. Mag.*, Vol. 29, No. 1, 124–135, 1993.

15. Zhu, Z., D. Howe, and C. Chan, "Improved analytical model for predicting the magnetic field distribution in brushless permanent-magnet machines," *IEEE Trans. Mag.*, Vol. 38, No. 1, 229–238, 2002.

16. Zarko, D., D. Ban, and T. Lipo, "Analytical calculation of magnetic field distribution in the slotted air gap of a surface permanent-magnet motor using complex relative air-gap permeance," *IEEE Trans. Mag.*, Vol. 42, No. 7, 1828–1837, 2006.

17. Jian, L., G. Xu, C. C. Mi, K. T. Chau, and C. C. Chan, "Analytical method for magnetic field calculation in a low-speed permanent-magnet harmonic machine," *IEEE Transactions on Energy Conversion*, Vol. 26, No. 3, 862–870, 2011.

18. Hwanga, C., C. Changa, C. Panb, and T. Changc, "Estimation of parameters of interior permanent magnet synchronous motors," *Journal of Magnetism and Magnetic Materials*, Vol. 239, Nos. 1–3, 600–603, 2006.

19. Lovelace, E., T. Jahns, and J. H. Lang, "A saturating lumped-parameter model for an interior PM synchronous machine," *IEEE Transactions on Industry Applications*, Vol. 38, No. 3, 645–650, 2002.

20. Mirahki, H. and M. Moallem, "Comparison of saturated parameters of three-layer interior permanent magnet synchronous machine obtained from lumped parameter model and finite element method," *21st Iranian Conference on in Electrical Engineering (ICEE)*, 1–5, 2013.

21. Chu, W. and Z. Zhu, "On-load cogging torque calculation in permanent magnet machines," *IEEE Trans. Mag.*, Vol. 49, No. 6, 2982–2989, 2013.

22. Zhu, L., S. Z. Jiang, Z. Zhu, and C. Chan, "Analytical modeling of open-circuit air-gap field distributions in multisegment and multilayer interior permanent-magnet machines," *IEEE Trans. Mag.*, Vol. 45, No. 8, 3121–3130, 2013.

23. Studer, C., A. Keyhani, T. Sebastian, and S. Murthy, "Study of cogging torque in permanent magnet machines," *Conference Record of the 1997 IEEE Industry Applications Conference, Thirty-Second IAS Annual Meeting, IAS' 97*, Vol. 1, 42–49, 1997.